

# A Multi-resolution Approach for Combining Visual Information using Nuclei Segmentation and Classification in Histopathological Images

Harshita Sharma<sup>1</sup>, Norman Zerbe<sup>2</sup>, Daniel Heim<sup>2</sup>, Stephan Wienert<sup>3</sup>, Hans-Michael Behrens<sup>2,4</sup>,  
Olaf Hellwich<sup>1</sup> and Peter Hufnagl<sup>2</sup>

<sup>1</sup>Computer Vision and Remote Sensing, Technische Universität Berlin, Marchstr.23, MAR 6-5, 10587, Berlin, Germany

<sup>2</sup>Department of Digital Pathology and IT, Institute of Pathology, Charité - Universitätsmedizin Berlin, Berlin, Germany

<sup>3</sup>VMscope GmbH, Berlin, Germany

<sup>4</sup>Department of Pathology, Christian-Albrechts University, Kiel, Germany

**Keywords:** Histopathology, H&E, Gastric Cancer, Nuclei segmentation, Virtual microscopy, Image analysis, Multi-resolution, AdaBoost.

**Abstract:** This paper describes a multi-resolution technique to combine diagnostically important visual information at different magnifications in H&E whole slide images (WSI) of gastric cancer. The primary goal is to improve the results of nuclei segmentation method for heterogeneous histopathological datasets with variations in stain intensity and malignancy levels. A minimum-model nuclei segmentation method is first applied to tissue images at multiple resolutions, and a comparative evaluation is performed. A comprehensive set of 31 nuclei features based on color, texture and morphology are derived from the nuclei segments. AdaBoost classification method is used to classify these segments into a set of pre-defined classes. Two classification approaches are evaluated for this purpose. A relevance score is assigned to each class and a combined segmentation result is obtained consisting of objects with higher visual significance from individual magnifications, thereby preserving both coarse and fine details in the image. Quantitative and visual assessment of combination results shows that they contain comprehensive and diagnostically more relevant information than in constituent magnifications.

## 1 INTRODUCTION

Gastric cancer is the fourth leading cancer and the second most common cause of cancer-related deaths worldwide. According to World Health Organization, it causes approximately 800,000 deaths each year. Gastric cancer is the accumulation of an abnormal group of cells, either malignant or cancerous, which form a tumor in the stomach (Nordqvist, 2013). Histologically, the most commonly occurring type of gastric malignancy is adenocarcinoma (90-95%), which starts in the mucous-producing cells on the inner lining of stomach and tends to invade the gastric wall aggressively, infiltrating muscularis mucosa, submucosa, and then muscularis externa. Some other types of gastric cancer include lymphomas (1-5%), gastrointestinal stromal tumor (2%), carcinoids (1%), adenoacanthomas (1%), and squamous cell carcinomas (1%) (Cabebe and Mehta, 2008).

Histological image analysis was initially explored

by Bartels (Bartels et al., 1992), Hamilton (Hamilton et al., 1994) and Weind (Weind et al., 1998), but has been a neglected area of research due to specialized acquisition process and lack of computational resources. However with rapid growth of computer-aided techniques, histological image analysis systems have seen recent developments. Most techniques utilize texture, color and morphological features on different kinds of histological images such as in (Shuttleworth et al., 2002a), (Diamond et al., 2004), (Roula et al., 2002), (Rani et al., 2010) for applications of cancer classification, grading or tissue analysis. However, performance of the state-of-the-art analysis techniques varies depending on datasets with specific magnification and malignancy levels, hence, is insufficient for heterogeneous histological datasets. Therefore, an appropriate improvement in this direction can be the use of multi-resolution methods. A multi-resolution texture analysis technique is used in (Shuttleworth et al., 2002b) for classifying colon cancer im-

ages that focuses on varying distances of texture co-occurrence matrix instead of spatial resolution, and does not include isolation of nuclei before classification. Our work, on the other hand, emphasizes on object-oriented classification of nuclei segments in gastric cancer images based on their texture, intensity and morphological characteristics. A multi-resolution approach is also reported in (Kong et al., 2009) for neuroblastoma images where higher magnification is considered only when the results from lower magnifications are unsatisfactory, using a feedback loop involving pathologists. It is intuitive that highest amount of useful information should be contained in higher magnifications, but it is also important to observe the ratio between the relevant and irrelevant information and how to differentiate between them. So we consider all resolutions simultaneously and perform visual and quantitative assessment to verify our assumption. Another related work reports a multi-class and two-stage classification of Wright stained WBCs (Ramesh et al., 2012). In the first stage, cells are classified as ones with segmented and non-segmented nucleus, and in the second stage as one of the five subtypes. We also address a similar classification problem, but use distinct classification approaches on gastric cancer images that differ in cell types and staining method. Further, we are motivated to work with gastric cancer specimens as negligible work has been done in their computer-based histological image analysis and it is still an emerging topic which needs to be explored.

Segmentation is a crucial and challenging step in most histological image analysis problems. Performance of subsequent tasks like feature extraction and classification largely depends on the results of the segmentation algorithm. It is difficult mainly due to the complex appearance of cells. When a tissue section is digitally scanned using a single focal plane, the scanner focuses on one two-dimensional layer in the region of interest, however, as the tissue section is three-dimensional it leads to unfocused neighboring cells, thereby creating overlaps and unclear cell boundaries in the resulting digital image. Another factor is the cutting direction during slide preparation. Hence, manual and automatic segregation of cell nuclei is a tedious process. Our work aims to address this challenge by using a multi-resolution approach to combine segmentation results at different magnifications in order to obtain better results for further analysis.

The human epidermal growth factor 2 (Her2) gene is a proto-oncogene whose high amplification causes a protein overexpression in cell membrane of a malignant cell, leading to abnormal cell division and

growth (Chua and Merrett, 2012). It has been most widely studied in breast cancers. Neu is a protein which is encoded by the Her2 gene in humans. Her2/neu has been recently introduced as a predictive biomarker for gastric cancer. Her2/neu staining involves higher costs and is still not common in laboratory practice. Haematoxylin and eosin (H&E) stain is used routinely in histological examinations because it provides a detailed view by clearly staining the tissue components, is simpler to apply and less costly (Bancroft and Gamble, 2008). For this study, Her2/neu and H&E stained images were available but we have developed our methods for H&E stained tissue sections because of their wider usability and lower preparation costs.

The organization of the paper is as follows: In section 2 we describe the methodology of our work. Section 3 describes the materials used, data preparation and technical details. Section 4 includes results and discussion, and Section 5 concludes the paper and presents the future directions of our research.

## 2 METHODOLOGY

### 2.1 System Overview

An overview of our system is provided in Figure 1. Firstly, the WSI specimens are registered to transform

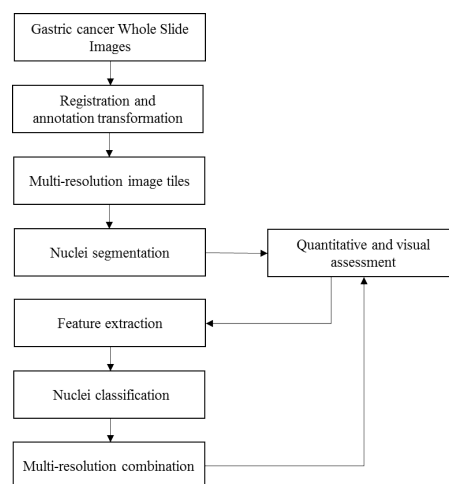


Figure 1: System overview.

annotations of pathologists from Her2/neu to H&E stain. This is followed by segmentation of nuclei components in H&E stained images, and their feature extraction. The features are used to train AdaBoost classification algorithm and results obtained are utilized to combine image data at different magnifica-

tions for enhanced segmentation results. The whole system is evaluated quantitatively and visually at different stages to assure its usability.

## 2.2 Image Registration

Our image dataset consists of surgical specimens in Her2/neu and H&E stains. Expert pathologists have annotated only the Her2/neu specimens (details in Section 3.1). Therefore, it is required to transform annotations of pathologists from Her2/neu slides into corresponding annotations in H&E slides for further experiments. Difference between slices in two stains is not negligible; hence corresponding WSI specimens are first registered semi-automatically. Using the registration information, coordinates of polygon annotations of pathologists from Her2/neu slide are transformed into destination coordinates in H&E slide using local affine transformation for all points inside a convex hull of point cloud, and global rigid transformation for all points lying outside the cloud, using Singular Value Decomposition method (Amidror, 2002). Different marked polygon areas from WSI specimens are tessellated at different magnifications ranging from 10x to 40x, the tile with highest magnification of size  $1024 \times 1024$ . As pathologists' annotations are not completely overlapping, the selected tissue areas are enclosed in maximum annotations, ensuring agreement of most pathologists to minimize inter-observer variability.

## 2.3 Nuclei segmentation

In the nuclei segmentation step, a minimum-model method consisting of six main steps (Wienert et al., 2012) is applied to isolate the nuclei at each magnification. It is a fully automatic approach, and yields a result like the one shown in Figure 2.

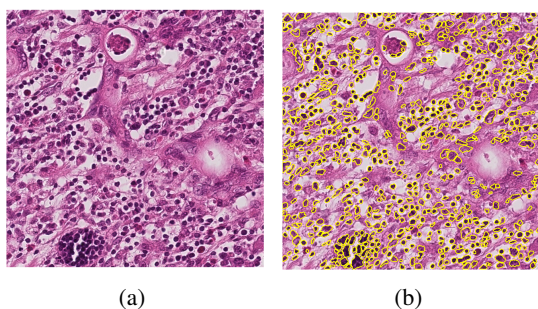


Figure 2: Nuclei segmentation result example at 25x magnification (a) Original image (b) Image showing nuclei segments.

## 2.4 Nuclei Feature Extraction

In this step, object-based feature extraction is performed where features are computed on image objects, in our case being the nuclei segments. A feature vector of 31 nuclei features based on color, texture and morphology are extracted from segments, as described below. A listing of the feature types considered in this work is summarized in Table 1.

### 2.4.1 Intensity-based Features

Intensity-based features are important for histological images due to the specific stains used. The features used to characterize the intensity of segments in our work include Mean Intensity, Mean Intensity on Contour, Standard Deviation of Intensity, Standard Deviation of Intensity on Contour (Hufnagl et al., 1984), Contour Value and Gradient Fit (Wienert et al., 2012). Mean Chromaticity is also calculated, where chromaticity for  $i^{th}$  RGB pixel  $\mathbf{p}_i$  is defined as the minimum euclidean distance  $d_{min}$  between pixel RGB value and points on the diagonal where each point  $\mathbf{p}_d$  is defined by RGB value  $R = G = B = x, x \in \{0, 1, ..255\}$ . In other words, it is the minimum euclidean distance of a pixel to a grey pixel value, as given in (1).

$$d_{min}(\mathbf{p}_i, \mathbf{p}_d) = \min(\|\mathbf{p}_i - \mathbf{p}_d\|) \quad \mathbf{p}_i, \mathbf{p}_d \in \mathbb{R}^3 \quad (1)$$

### 2.4.2 Morphological Features

Shape or morphological properties are used by pathologists to identify or distinguish between different types of nuclei components. In our experiments, we use the following morphological features: Object Pixels, Minimum Distance to Tessellation Border, Pixels at Layer Border, Maximum Distance to Border, Aspect Ratio of Bounding Ellipsoid, Minor Axis of Bounding Ellipsoid, Major Axis of Bounding Ellipsoid, Angle of Bounding Ellipsoid, Form Factor of Contour, Convexity of Contour, Length of Contour, Area of Contour, Form Factor of Convex Hull, Length of Convex Hull, Area of Convex Hull (Hufnagl et al., 1984), Feret, Minimal Radius of Enclosing Centered Circle, Maximal Radius of Enclosed Centered Circle, Roundness and Form Factor (Zerbe, 2008).

### 2.4.3 Texture Features

Texture is also a widely used characteristic in histological image analysis, and varies with different tissue components. We have selected the features contrast, energy, entropy and homogeneity to represent texture of nuclei segments. These are a subset of the Haralick GLCM features (Haralick et al., 1973).

Table 1: Summary of nuclei features.

Feature type	Number of features
Intensity-based	7
Morphological	20
Texture	4
Total	31 nuclei features

## 2.5 AdaBoost Classification

The segments are automatically classified into eight different classes using AdaBoost classification method (Bishop, 2006) (See Figure 4 for description of nuclei classes). A multi-class AdaBoost classification algorithm has been developed for this task. AdaBoost or Adaptive Boosting is the most widely used form of boosting. Boosting involves ensemble learning where a collection of component classifiers or learners is used and a joint decision is taken by combining their predictions. AdaBoost allows adding

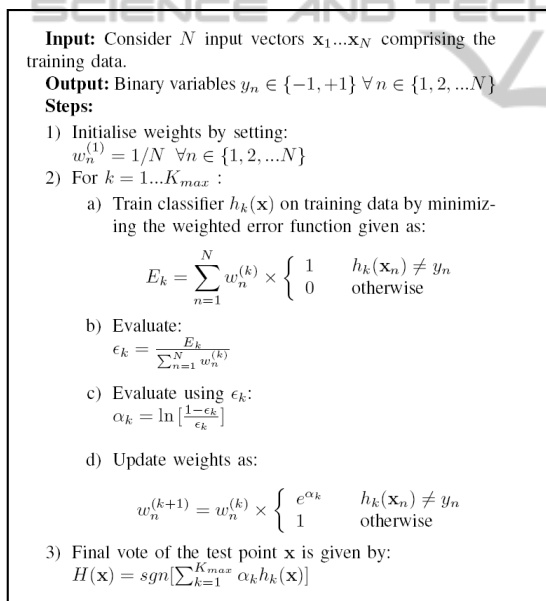


Figure 3: AdaBoost algorithm.

a sequence of weak learners to the algorithm, until a desired low training error is achieved. Each weak learner corresponds to a simple decision stump. The ensemble of weak learners can be defined as  $h_k(\mathbf{x}), k = 1, 2, \dots, K_{max}$ , where  $K_{max} = 15$  is used in our algorithm. The strong learner is assembled from all weak learners through a weighted majority voting scheme. The AdaBoost algorithm for a two-class classification problem is given in Figure 3.

We extend the two-class classification algorithm to multi-class by considering the final vote as the class

with majority votes of weighted binary learners. A boosting algorithm like AdaBoost involving a combination of classifiers is proposed as a new direction for improving performance of individual classifiers like kNN, Naive Bayes and SVM (Kotsiantis et al., 2007). AdaBoost is also found to be easier to implement than other maximal margin classifiers like SVM. Further, SVM is not robust to irrelevant descriptors, hence, not suitable to use without feature selection (Chen and Lin, 2006), however our method considers all 31 nuclei features equally. This explains the choice of initially selecting the AdaBoost algorithm for the classification task. A comparison of the performance of different classification methods on our image dataset is beyond the scope of the work presented in this paper and a recognized future direction.

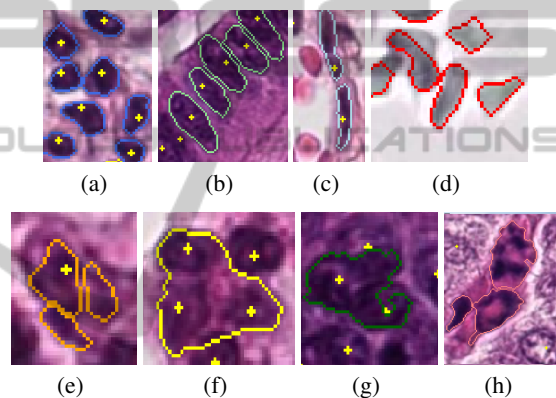


Figure 4: Examples of segments with defined nuclei classes (a) Leukocytes (b) Epithelial nuclei (c) Fibrocytes/border cells (d) Other nuclei (including blood cells in vessel) (e) Nuclei fragments (f) Cluster of nuclei (g) Badly segmented nucleus (h) Artefacts.

Definitions of the multiple nuclei classes have been previously approved by pathologists. These are leukocyte, epithelial nucleus, fibrocyte/border cell, other nuclei (including blood cells in vessel), cluster of nuclei, nuclei fragment, badly segmented nucleus and artefact. Figure 4 illustrates the nuclei classes.

In order to obtain optimum results, we have evaluated two classification approaches. The first approach performs a single stage classification of segments into one of the eight classes. In the second approach, a two-stage classification is performed. The first stage classifies the segments into three broad classes namely compact objects including epithelial nuclei, leukocytes, fibrocytes/border cells, other nuclei and nuclei fragments; conglomerates including clusters of nuclei and badly segmented nuclei, and artefacts. In the second stage, each class objects are further classified into one of the respective subclasses. Figure 5 shows the hierarchy of classes used in this approach.

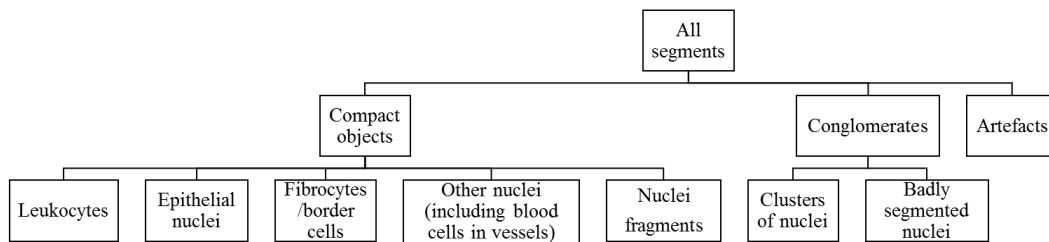


Figure 5: Hierarchy of classes in multi-stage classification approach.

## 2.6 Multi-resolution Combination

To combine the segmentation results of different magnifications, the procedure depicted in Figure 6 is used. A relevance score is assigned to each segment de-

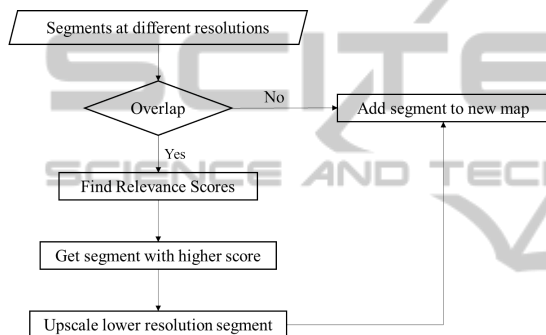


Figure 6: Multi-resolution combination method.

Table 2: Relevance scores.

Class	Diagnostic significance	Relevance Score
Epithelial nucleus	Highest	100
Leukocyte	Very high	80
Cluster of nuclei	High	60
Fibrocyte/border cell	Medium high	50
Other nuclei	Medium	20
Nuclei fragment	Medium low	10
Badly segmented nucleus	Low	5
Artefact	Lowest	0

pending on its class. The scoring is relative, depending on which information is visually more significant for diagnostic purpose, as given in Table 2. A new segmentation map is obtained with segments of higher visual importance from individual constituent magnifications. It should be specified that a map is a data structure that is used to store spatial positions of image objects after segmentation. It encapsulates a two dimensional array of unsigned integers that has

the size of the input image, where the unsigned integers are the identifiers of the corresponding segment of a given pixel. The segmentation map has the highest resolution, and contours of lower magnification are upscaled and added to the map. Hence, by using the classification results of segments at different magnifications, a more accurate combined segmentation result is obtained, containing more useful information than individual ones.

## 3 EXPERIMENTS

### 3.1 Materials

Her2/neu immunohistochemically stained and H&E stained surgical specimens of 12 cases (one specimen per case) were selected from a previous study of 483 cases of gastric cancer, acquired from proximal or distal parts of stomach. These were scanned using a Leica SCN400 microscopic whole-slide scanner at its maximum, nominally 400 times magnification with pixel size  $0.0676 \mu m^2$ . Whole slide images were exported from the scanner system into files of SCN format, which is a multi-image, pyramidal multi-resolution 64-bit TIFF format. Example of a typical Her2/neu stained WSI is shown in Figure 7.

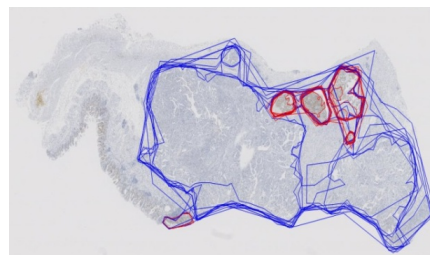


Figure 7: Example of a Her2/neu stained gastric cancer WSI specimen containing pathologists' annotations.

Each Her2/neu WSI specimen contains polygon annotations made by ten expert pathologists. These consist of Her2/neu positive areas marked by using the 10% cut-off rule (Warneke et al., 2013), with the

help of a digital microscopy software. The annotations also contain Her2/neu negative areas those were morphologically identified as tumor areas in the tissue by pathologists. Her2/neu positive areas define a high degree of malignancy, whereas Her2/neu negative areas denote a low malignancy level. The remaining areas of the tissue are widely necrotic tissue regions.

### 3.2 Dataset Preparation

The WSI specimens were acquired in SCN format and the corresponding annotations in vmpi01 format. Size of each whole slide image file is approximately 3 GB. The SCN files were converted into VSF (Virtual Slide Format) and the corresponding annotations to vmsm files which are XML-formatted metafiles containing metadata about the slides, one of them being annotations. These data formats are suitable for accessing whole slide image data using the VMscope software support (VMscope GmbH, 2010). CognitionMaster (Wienert et al., 2013), an object-oriented analysis framework, has been used for user interaction with tissue images, especially to create ground truth data for segmentation evaluation and training data for classification purpose.

### 3.3 Technical Details

Different modules of our methodology have been implemented in C# programming language, and tested on a system with Intel Core i7-3700 processor at 3.40 GHz and with 16 GB RAM. The total processing time for the training and classification steps is around 15-20 minutes for a training dataset containing approximately 6000 nuclei segments, using the AdaBoost classification algorithm. Each of the segmentation and multi-resolution combination steps requires less than a minute for a tile of size 1024 x 1024 pixels.

## 4 RESULTS AND DISCUSSION

### 4.1 Result Overview

Nuclei segmentation results of different magnifications from 10x to 40x are quantitatively and visually analyzed. Desired results are observed for the higher magnification 30x and full magnification 40x. It is also observed that there is a transition from clustering to fragmentation as we proceed from lower to higher magnifications. Two classification approaches have been evaluated. An average multi-class accuracy of 57.5% is achieved in the single stage approach and 58.8% for the multi-stage approach. The first stage of

multi-stage approach classifies compact objects (including cell nuclei), conglomerates and artefacts with an average accuracy of 85.6%, as required for our task. Quantitative and qualitative analysis of combined segmentation results shows that they contain more comprehensive information than individual constituent magnifications.

### 4.2 Nuclei Segmentation Evaluation

To evaluate the performance of the segmentation algorithm on the given dataset at different magnifications, five slides of varying stain intensities were initially selected for segmentation. 15 tiles per slide were selected with different degrees of malignancy, using pathologists' annotations. The nuclei were manually located with point annotations to create Ground Truth which was verified by expert pathologists. The tiles were annotated at highest resolution (40x). Each tile was automatically segmented at the selected magnifications of 10x, 15x, 20x, 25x, 30x, and 40x. The segmentation results were compared against the ground truth data. The following quantities were measured and compared: total number of manual annotations, number of segments found, number of nuclei correctly segmented, number of nuclei not segmented, number of segments not nuclei and number of clusters. This comparison was done at three levels: tile, slide and overall. Images containing point annotations and contours of segments formed automatically were also created for visual inspection and comparison. The overall result can be summarized in the graph in Figure 8.

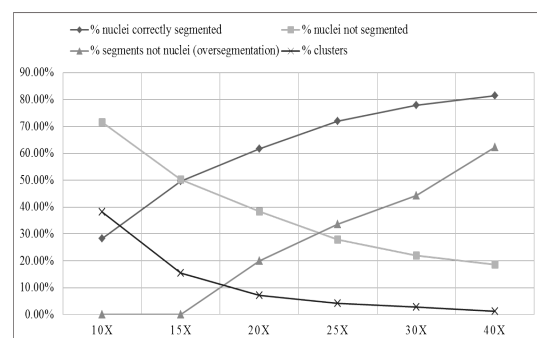


Figure 8: Nuclei segmentation performance at individual magnifications.

From the results of the described coarse to fine segmentation analysis, we observe that the percentage of correctly segmented nuclei increases with magnification. These are found by counting the segments which also contain point annotations and are marked as nuclei in the ground truth data. Also, oversegmen-

Table 3: Single stage classification: 30x.

	Leukocyte	Epithelial nucleus	Fibrocyte/ border cell	Nuclei Fragment	Other nuclei	Cluster of nuclei	Badly segmented nucleus	Artefact	All classes
Round1	75.00%	69.82%	59.69%	46.86%	29.61%	63.31%	16.36%	33.90%	<b>55.71%</b>
Round2	80.47%	72.24%	60.12%	44.62%	28.74%	56.89%	13.46%	24.37%	<b>56.52%</b>
Round3	81.79%	76.15%	62.61%	50.60%	23.81%	55.78%	16.67%	25.38%	<b>58.09%</b>
<b>Overall</b>	<b>79.20%</b>	<b>72.70%</b>	<b>60.80%</b>	<b>47.40%</b>	<b>27.55%</b>	<b>58.50%</b>	<b>15.61%</b>	<b>27.79%</b>	<b>56.78%</b>

Table 4: Single stage classification: 40x.

	Leukocyte	Epithelial nucleus	Fibrocyte/ border cell	Nuclei Fragment	Other nuclei	Cluster of nuclei	Badly segmented nucleus	Artefact	All classes
Round1	81.42%	75.24%	60.74%	47.37%	38.12%	51.38%	14.49%	40.98%	<b>57.80%</b>
Round2	77.59%	74.71%	67.74%	48.50%	35.16%	55.56%	16.98%	36.36%	<b>58.69%</b>
Round3	78.29%	77.71%	59.53%	49.85%	39.92%	53.33%	26.09%	40.63%	<b>58.43%</b>
<b>Overall</b>	<b>79.10%</b>	<b>75.90%</b>	<b>62.50%</b>	<b>48.60%</b>	<b>37.84%</b>	<b>53.48%</b>	<b>18.45%</b>	<b>39.38%</b>	<b>58.31%</b>

tation (segments not nuclei) increases with magnification. It has been calculated for an image using (2).

$$N_{ns} = N_t - N_s \quad (2)$$

where  $N_{ns}$  denotes number of segments not nuclei,  $N_t$  is the total number of segments found and  $N_s$  is the number of segmented nuclei. No oversegmentation for 10x and 15x magnifications indicates that the number of nuclei are equal to or greater than the number of segments, which means that same segment corresponds to one or more manually annotated nuclei. The number of clusters, which are segments containing more than one point annotation, decrease with magnification. In order to preserve the fine details in images, and to capture the maximum number of nuclei correctly identified, one choice is the full magnification 40x. However, to deal with the problem of oversegmentation and fragmentation evident mostly in 40x, it should be combined with a lower magnification to get more accurate results. For identifying which of the lower magnifications is suitable for combining with 40x, a pairwise comparison of results was made between 40x and each of the lower magnifications. The aim was to find the percentage of correctly segmented nuclei in lower magnifications which can contribute to the total correctly segmented nuclei in addition to 40x. It is calculated as given in (3).

$$\text{Additional contribution of } X = (N_{sx} - N_{sc}) / N_m \quad (3)$$

where  $N_{sx}$  denotes the number of correctly segmented nuclei found at magnification X,  $N_{sc}$  is the number of correctly segmented nuclei common in magnification X and 40x, and  $N_m$  is the number of manually annotated nuclei in the image. It is found almost equal

( $\approx 5\%$ ) for magnifications between 15x to 30x. It is lower for 10x ( $\approx 4\%$ ). The other factor used for deciding the other magnification is clustering. It is already found that clustering decreases with magnification. In order to minimize it, we select the next magnification with minimum clusters (2.8%) i.e. 30x.

Thus, after evaluating the results of nuclei segmentation algorithm it was concluded that segmentation information at 30x and 40x will be utilized for further analysis. Combining information at the level of segmentation itself is a non-trivial task, due to which automatic classification of segments was required to be performed.

### 4.3 Classification Evaluation

One half of the segmented data was manually classified to prepare the training dataset, making a total of 33 image tiles from five WSI specimens in each magnification 30x and 40x, selected such that they contain noticeable variation in stain and malignancy level. A total of 5541 segments in 30x and 5730 segments in 40x were used for training the classification algorithm. A 3-fold cross validation was performed to validate the classification using both approaches, with two-third segments considered as training data and remaining one-third as test data in every round. We ensured that there was no overlap between the training and test data in each round. Validation results were averaged over rounds and over classes.

We have compared the performance of the two classification approaches. Table 3 and Table 4 show the round-wise and overall accuracy using the first approach for 30x and 40x respectively. Using the second

approach, the first stage accuracy for 30x is given in Table 5 and for 40x in Table 6. The combined accuracy using this approach, after applying the two stages in sequence (considering the error of the first stage), is summarized in Table 7 and Table 8.

Table 5: First stage of multi-stage classification: 30x.

	Compact objects	Conglomerates	Artefacts	All classes
Round1	95.28%	51.63%	17.19%	<b>84.79%</b>
Round2	94.44%	57.71%	18.18%	<b>86.36%</b>
Round3	97.46%	52.38%	16.43%	<b>86.19%</b>
<b>Overall</b>	<b>95.71%</b>	<b>53.83%</b>	<b>17.17%</b>	<b>85.78%</b>

Table 6: First stage of multi-stage classification: 40x.

	Compact objects	Conglomerates	Artefacts	All classes
Round1	96.14%	52.70%	29.44%	<b>86.49%</b>
Round2	95.48%	53.99%	26.14%	<b>85.55%</b>
Round3	95.40%	51.45%	28.72%	<b>84.61%</b>
<b>Overall</b>	<b>95.68%</b>	<b>52.69%</b>	<b>28.13%</b>	<b>85.55%</b>

On comparing the performance of the two approaches (shown in Figure 9), we observe that the overall performance is better for the multi-stage approach. In both approaches, the recognition rate for leukocyte class is highest, followed by epithelial nuclei and fibrocytes/border cells, showing the compactness of the classes and ability of our classification method to strongly distinguish them based on the extracted feature set. However, for three classes namely leukocytes, clusters of nuclei and artefacts, single stage approach performs better than multi-stage approach. Poor performance is observed for the class other nuclei, which can be explained as they contain nuclei not visually clear in the images to be distinguished into a specific class and also include blood cells in vessels, which have a very low occurrence. Artefacts also have a lower recognition rate due to lower number of instances, and absence of a well-defined visual appearance. An average accuracy for clusters could be explained by lower number of samples in the training dataset. The reason for a lower accuracy of clusters in the multi-stage approach is due to lower first stage accuracy of conglomerate class, however it is to be specified that the second stage accuracy for clusters is comparatively high ( $\approx 88\%$ ), hence ways to improve first stage accuracy of class conglomerates should be developed. We also note for the second approach, the first stage accuracy is relatively high for the compact objects class i.e. 95.7%, which is a desired characteristic, as visually important segments will be present mostly in this class. The nu-

clei fragments have a similar appearance with other nuclei, and we also observe from generated confusion matrices that they are misclassified as one of the other compact objects in the second stage. In general, the multi-stage approach has an overall better and more stable performance and also the advantage of providing a broad classification of segments using the first classification stage, hence it outweighs the single stage approach and we have considered it for further experiments.

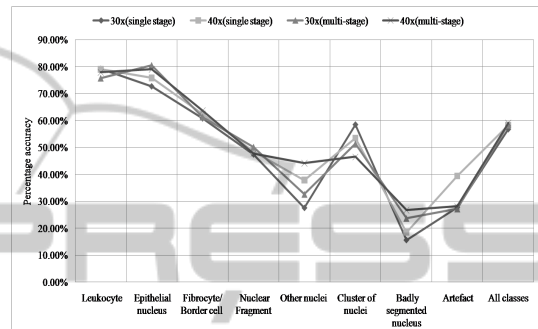


Figure 9: Single stage vs. multi-stage classification approach.

#### 4.4 Multi-resolution Combination Evaluation

The results of multi-resolution combination were evaluated using the method described in Section 4.2. The overall combination result can be summarized in Figure 10. From the quantitative and visual evaluation of the multi-resolution combination method, we observe that the results are superior to individual magnifications. Quantitatively, the percentage of correctly segmented nuclei for combined results is higher and percentage of nuclei not segmented is lower than in each magnification 30x and 40x, showing the contribution of segmented nuclei from both magnifications. The percentage of clusters is also reduced. By visual assessment of our results, we find that some nuclei fragments in 40x have been replaced with corresponding whole nuclei from 30x. Similarly, some clusters in 30x are also replaced with individual nuclei in 40x.

However, one undesirable effect observed is the number of segments not counted as nuclei (considered as oversegmentation) is slightly higher for combination. A primary reason for this behavior is the presence of fragments in this category, which do not enclose point annotations denoting individual nuclei in ground truth, and which have been retained due to their misclassification as other types of nuclei within the compact objects class. Dealing with this problem and also finding a solution to handle nuclei fragments

Table 7: Both stages of multi-stage classification: 30x.

	Leukocyte	Epithelial nucleus	Fibrocyte/ border cell	Nuclei Fragment	Other nuclei	Cluster of nuclei	Badly segmented nucleus	Artefact	All classes
Round1	76.83%	80.97%	60.16%	54.85%	34.47%	53.01%	20.96%	17.19%	<b>59.38%</b>
Round2	72.48%	82.04%	60.07%	43.65%	30.31%	46.93%	28.16%	18.18%	<b>56.84%</b>
Round3	77.75%	78.17%	63.75%	51.98%	32.95%	54.40%	20.88%	16.43%	<b>58.51%</b>
<b>Overall</b>	<b>75.69%</b>	<b>80.45%</b>	<b>61.29%</b>	<b>50.13%</b>	<b>32.61%</b>	<b>51.38%</b>	<b>23.68%</b>	<b>17.17%</b>	<b>58.48%</b>

Table 8: Both stages of multi-stage classification: 40x.

	Leukocyte	Epithelial nucleus	Fibrocyte/ border cell	Nuclei Fragment	Other nuclei	Cluster of nuclei	Badly segmented nucleus	Artefact	All classes
Round1	77.48%	83.54%	66.80%	44.21%	41.53%	49.07%	23.42%	29.44%	<b>59.17%</b>
Round2	80.31%	75.73%	61.76%	47.19%	44.38%	47.99%	28.28%	26.14%	<b>58.43%</b>
Round3	75.96%	77.94%	62.66%	52.36%	46.71%	43.00%	29.78%	28.72%	<b>59.38%</b>
<b>Overall</b>	<b>77.91%</b>	<b>79.10%</b>	<b>63.69%</b>	<b>47.79%</b>	<b>44.22%</b>	<b>46.52%</b>	<b>26.74%</b>	<b>28.13%</b>	<b>59.15%</b>

or clusters in both magnifications is a future direction of our research.

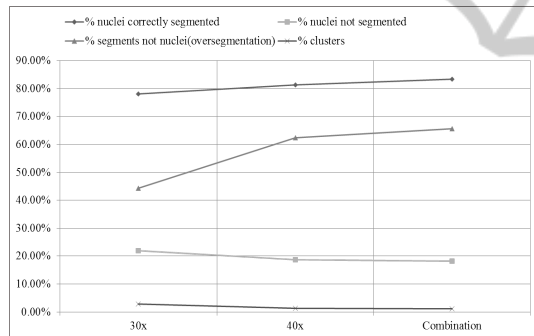


Figure 10: Nuclei segmentation performance of combined result vs. individual magnifications 30x and 40x.

## 5 CONCLUSIONS

In this paper, we have achieved improved nuclei segmentation results from different magnifications by combining their diagnostically useful and eliminating their undesirable information, in haematoxylin and eosin stained gastric cancer WSI specimens. In our experiments, we have used a comprehensive dataset of slides having different degrees of H&E stain. Further, polygon areas marked by expert pathologists using Her2/neu immunohistochemical staining, define varying levels of malignancy in the tissue. Hence, our experimental results show that the approach can be useful for deriving visual information from heterogeneous datasets, varying in degree of stain and ma-

lignancy. It should be noted that this paper presents preliminary results of our baseline method.

Such visual information fusion will further assist computer-aided analysis of cancer images which can help pathologists in diagnosis-related tasks. Classification accuracy can be improved by increasing data size and incorporating neighbourhood information of segments. In future, we aim to work in this direction by using more sophisticated topological features, including graph-theoretic description of gastric cancer images. We also plan to perform a comparative analysis of various classification techniques on our dataset and evaluate the performance of our methods on other types of cancers. The focus is to retrieve and classify tissue sections in a reliable way.

## ACKNOWLEDGEMENTS

This work is supported with funds from the German Academic Exchange Service (DAAD). The authors are grateful to the Department of Pathology, Christian-Albrechts University, for providing gastric cancer WSI specimens for this study, especially Dr.Christine Böger for performing review of the training data. We thank Mr.Björn Lindequist, Charité for his contribution in the pre-processing stage. We also thank Dr.Fredrich Klauschen, Charité for giving valuable suggestions on histological architecture to form classes for subsequent analysis, and Ms.Iris Klemper, Charité for reviewing point annotations of nuclei in ground truth data. We sincerely thank VMscope GmbH for providing suitable software tools to access whole slide image data as required for our work.

## REFERENCES

- Amidror, I. (2002). Scattered data interpolation methods for electronic imaging systems: a survey. *J. Electronic Imaging*, 11(2):157–176.
- Bancroft, J. D. and Gamble, M. (2008). *Theory and practice of histological techniques*. Elsevier Health Sciences.
- Bartels, P., Thompson, D., Bibbo, M., and Weber, J. (1992). Bayesian belief networks in quantitative histopathology. *Anal Quant Cytol Histol*, 14(6):459–73.
- Bishop, C. M. (2006). *Pattern Recognition and Machine Learning (Information Science and Statistics)*. Springer-Verlag New York, Inc., Secaucus, NJ, USA.
- Cabebe, E. C. and Mehta, V. K. (2008). Gastric cancer. <http://emedicine.medscape.com/article/278744-overview#showall>.
- Chen, Y. W. and Lin, C. J. (2006). Combining SVMs with various feature selection strategies. In *Feature extraction*, pages 315–324. Springer.
- Chua, T. and Merrett, N. (2012). Clinicopathologic factors associated with HER2-positive gastric cancer and its impact on survival outcomes—a systematic review. *Int J Cancer*, 130(12):2845–56.
- Diamond, J., Anderson, N., Bartels, P., Montironi, R., and Hamilton, P. (2004). The use of morphological characteristics and texture analysis in the identification of tissue composition in prostatic neoplasia. *Human Pathology*, 35(9):1121–1131.
- Hamilton, P., Anderson, N., Bartels, P., and Thompson, D. (1994). Expert system support using bayesian belief networks in the diagnosis of fine needle aspiration biopsy specimens of the breast. *J Clin Pathol*, 47(4):329–36.
- Haralick, R. M., Shanmugam, K. S., and Dinstein, I. (1973). Textural features for image classification. *IEEE Transactions on Systems, Man and Cybernetics*, 3(6):610–621.
- Hufnagl, P., Schlosser, A., and Voss, K. (1984). Merkmale der Form, Größe und Lage digitaler objekte. *Bild und Ton.*, 37:293–298.
- Kong, J., Sertel, O., Shimada, H., Boyer, K. L., Saltz, J. H., and Gurcan, M. N. (2009). Computer-aided evaluation of neuroblastoma on whole-slide histology images: Classifying grade of neuroblastic differentiation. *Pattern Recogn.*, 42(6):1080–1092.
- Kotsiantis, S. B., Zaharakis, I., and Pintelas, P. (2007). Supervised machine learning: A review of classification techniques. In *Emerging Artificial Intelligence Applications in Computer Engineering*, pages 3–24. IOS Press.
- Nordqvist, C. (2013). What is Stomach Cancer? What is Gastric Cancer? *Medical News Today. MediLexicon, Intl.* <http://www.medicalnewstoday.com/articles/257341.php>.
- Ramesh, N., Dangott, B., Salama, M. E., and Tasdizen, T. (2012). Isolation and two-step classification of normal white blood cells in peripheral blood smears. *Journal of pathology informatics*, 3.
- Rani, S., Kannammal, A., Nirmal, M., Prabhu, K., and Kumar, R. (2010). Multi-feature prostate cancer diagnosis of histological images using advanced image segmentation. *IJMEI*, 2(4):408–416.
- Roula, M., Diamond, J., Bouridane, A., Miller, P., and Amira, A. (2002). A multispectral computer vision system for automatic grading of prostatic neoplasia. In *Proceedings IEEE International Symposium on Biomedical Imaging*, pages 193–196.
- Shuttleworth, J., Todman, A., Naguib, R., Newman, B., and Bennett, M. (2002a). Colour texture analysis using co-occurrence matrices for classification of colon cancer images. In *IEEE Canadian Conference on Electrical and Computer Engineering*, volume 2, pages 1134–1139.
- Shuttleworth, J., Todman, A., Naguib, R., Newman, B., and Bennett, M. (2002b). Multiresolution colour texture analysis for classifying colon cancer images. In *Medicine and Biology, 24th Annual Conference and the Annual Fall Meeting of the Biomedical Engineering Society EMBS/BMES, Proceedings of the Second Joint*, volume 2, pages 1118,1119.
- VMscope GmbH (2010). Vmscope products. <http://vmscope.com/produkte.html>.
- Warneke, V. S., Behrens, H., Böger, C., Becker, T., Lordick, F., Ebert, M., and Röcken, C. (2013). Her2/neu testing in gastric cancer: evaluating the risk of sampling errors. *Annals of Oncology*, 24(3):725–733.
- Weind, K., Maier, C., Rutt, B., and Moussa, M. (1998). Invasive carcinomas and fibroadenomas of the breast: comparison of microvessel distributions—implications for imaging modalities. *Radiology*, 208(2):477–83.
- Wienert, S., Heim, D., Kotani, M., Lindequist, B., Stenzinger, A., Ishii, M., Hufnagl, P., Beil, M., Dietel, M., Denkert, C., and Klauschen, F. (2013). Cognitionmaster: an object-based image analysis framework. *Diagnostic Pathology*, 8(1):1–8.
- Wienert, S., Heim, D., Saeger, K., Stenzinger, A., Beil, M., Hufnagl, P., Dietel, M., Denkert, C., and Klauschen, F. (2012). Detection and segmentation of cell nuclei in virtual microscopy images: A minimum-model approach. *Scientific Reports*, 2.
- Zerbe, N. (2008). Analyse serieller histologischer Schnitte im Hinblick auf die automatische Bestimmung gleichartiger Partikel benachbarter Schnittstufen. Diplomarbeit, Fachhochschule für Technik und Wirtschaft Berlin.